J|A|C|S
ARTICLES
Published on Web 08/15/2002

Chemical Bonding Variations and Electron−Phonon Interactions

Shuiquan Deng, Arndt Simon,* and Jürgen Köhler

Contribution from the Max-Planck-Institut für Festkörperforschung, Heisenbergstrasse 1, D-70569 Stuttgart, Germany

Received July 26, 2001. Revised Manuscript Received November 5, 2001

Abstract: A new functional, Psib(Φ), of an electronic state in solids based on the bonding indicator $B(\tau,\tau')$ in terms of Mulliken's electron partitioning approach has been introduced. Using Psib(Φ), the bonding variations of an electronic state caused by electron−phonon coupling can be studied. With this proposed approach, the differences between the "flat band" states for Hg in coupling to the phonons and the peaklike structure of electron−phonon coupling constants in the **q** space are well explained.

Introduction

In exploring the connection between superconductivity and chemistry, we have proposed a "flat band−steep band" scenario for the occurrence of superconductivity based on the chemical origin of pairwise attractive interaction between conduction electrons.[1] In this model, the coexistence of bands with large dispersion and bands with vanishing slope at the Fermi level is essential. This scenario bears some similarity with the "itinerant electrons versus local pair" model[2] also applied to high-T_C cuprates. However, our model is based on the actual band structures extracted from first principles, which is not necessarily equivalent to a two-band model. Through testing the model for Hg[3] and Ca,[4] we have established the approach to determine the "flat band" and "steep band" in the entire first Brillouin zone. The interplay between the high-velocity electrons and nearly zero-velocity electrons are realized through the interactions with those phonons, which provide significant electron−phonon coupling. In our previous work, we studied the coupling between the electrons and specific phonons with the linear response approach. By using the extended degenerate perturbation theory, we have demonstrated the correspondence between the electron−phonon interactions and the "dynamic pseudo Jahn−Teller effect".[5] In this work, we will study the behavior and particularly the bonding variations of the flat band states caused by specific phonons.

Description of Method

Within the ab initio framework, the behavior of a specific electronic state in a phononic field can be studied through the linear response theory.[6,7] or the frozen phonon approach.[8] The former approach can deal with any phonons; however, it does not fully consider the anharmonic effects. The latter one overcomes this difficulty; however, it is normally limited to the high symmetric and commensurate phonon modes corresponding to supercells of appropriate sizes. In this work, the frozen phonon approach is used because the variation of a wave function caused by a specific phonon can easily be obtained in this approach.

A phonon mode can be viewed as a dynamic displacement field $\mathbf{u}_{l\kappa}$ acting on the equilibrium structure, $\mathbf{x}_{l\kappa} = \mathbf{x}^0_{l\kappa} + \mathbf{u}_{l\kappa}$, where $\mathbf{x}^0_{l\kappa}$ indicates the equilibrium position of the κth atom in the **l***th* unit cell; $\mathbf{u}_{l\kappa}$ can be calculated from the following formula:

$$\mathbf{u}_{l\kappa} = \frac{A_{qj}}{\sqrt{m_\kappa}} \mathrm{e}^{qj}_\kappa \exp(iq\mathbf{x}^0_{l\kappa} - i\omega_{qj}t) \qquad (1)$$

where A_{qj} is the amplitude of the vibration, m_κ the mass of the κth atom, $\mathbf{e}^{qj}_\kappa$ the polarization vector, and ω_{qj} the frequency. The amplitude of a phonon at very low temperature can be calculated based on the Debye temperature θ_D as follows,[9]

$$\langle \mathbf{u}_{l\kappa}{}^2 \rangle = 9\hbar^2/4m_\kappa k_B \theta_D \qquad (2)$$

where k_B is the Boltzmann constant. The polarization vector $\mathbf{e}^{qj}_\kappa$ can be obtained from symmetry analysis[10] or from linear response calculations. Applying $\mathbf{u}_{l\kappa}$ at an arbitrary time t, e.g. $t = 0$, on a structure is equivalent to modulating it by a displacement wave of wave vector **q** of a phonon, and accordingly, a specific electronic state $|\mathbf{k}j\rangle$ will be transformed

* To whom correspondence should be addressed. E-mail: simon@sim.mpi-stuttgart.mpg.de.

(1) Simon, A. *Angew. Chem., Int. Ed. Engl.* **1997**, *36*, 1788.
(2) Micnas, R.; Ranninger, J.; Robaszkiewicz, S. *Rev. Mod. Phys.* **1990**, *62*, 113.
(3) Deng, S.; Simon, A.; Köhler, J. *Angew. Chem., Int. Ed. Engl.* **1998**, *37*, 640.
(4) Deng, S.; Simon, A.; Köhler, J. *Solid State Sci.* **2000**, *2*, 31.
(5) Deng, S.; Simon, A.; Köhler, J. *J. Phys. Chem. Solids* **2001**, *62*, 1441.
(6) Baroni, S.; Giannozzi, P.; Testa, A. *Phys. Rev. Lett.* **1987**, *58*, 1861.
(7) Savrasov, S. Y. *Phys. Rev. B* **1996**, *54*, 16470.
(8) Wendel, H.; Martin, R. M. *Phys. Rev. B* **1979**, *19*, 5251.
(9) Reissland, J. A. *The Physics of Phonons*; John Wiley & Sons Ltd.: London, 1973; p 134. Kunc, K.; Martin R. M. *Ab Initio Calculation of Phonon Spectra*; Devreese, J. T., Van Dorean, V. E., Van Camp, P. E., Eds.; Plenum Press: New York, 1983; p 65.
(10) Montgomery, H. *Proc. R. Soc. A* **1969** *309*, 521.

10.1021/ja011815q CCC: $22.00

into $|\mathbf{k} \pm \mathbf{q}j'\rangle$. Two calculations based on the original unit cell and the supercell, respectively, are performed, where **k** is the wave vector of an electron and j is the band index.

To see the variation in bonding involved in this process we need a bonding indicator for a specific electronic state in a solid. As the existing bonding indicators such as COHP[11] embedded in the tight-binding linear muffin-tin orbital (TB-LMTO)[12] scheme and COOP[13] embedded in the *extended Hückel* (EH)[14] scheme are based on the *density of states* (DOS), they cannot be used directly in our case. Considering a solid as a large molecule,[15] we can treat a one-electron wave function as a molecular wave function. Suppose that we have a band state $|\mathbf{k}j\rangle$ which can be expanded in terms of some kind of basis set $|\chi_\alpha^{\mathbf{k}}\rangle$,

$$|\mathbf{k}j\rangle = \sum_\alpha |\chi_\alpha^{\mathbf{k}}\rangle C_\alpha^{\mathbf{k}j} \tag{3}$$

where α runs over all freedoms of the basis functions, for example, in the full potential LMTO (FP-LMTO) method,[16] α is just a shorthand notation of τ, κ, L, with τ representing the position vectors of atoms in the primitive unit cell, $\epsilon = \kappa^2$ being the energy parameter to represent the tail energy of the envelop function, and L the combination of the angular momentum quantum numbers l (0, 1, 2, ...) and m ($-$l, $-$l + 1, ... l $-$ 1, l). After the energy freedom in α of (3) is summed out, the expansion formula (3) is similar to the linear combination of atomic orbitals into a molecular orbital. Therefore, we can devise a Mulliken[17] bonding indicator in a solid. Mulliken's idea is that as $\psi^2(\mathbf{r})\,d\mathbf{r}$ can be explained as the probability of an electron appearing in a microvolume d**r**. The probability that an electron occurs between two atoms can be taken as a measure for a bond order, and thus, the normalization condition of a wave function naturally corresponds to the total probability in the entire space. Now we start from (3) by assuming that the energy dependence of the basis functions has been summed out. The **k** dependence of $|\chi_\alpha^{\mathbf{k}}\rangle$ is due to the Bloch law as shown in the following:

$$\chi_{\tau,L}^{\mathbf{k}}(\mathbf{r}) = \sum_{\mathbf{R}} e^{i\mathbf{k}\mathbf{R}} \chi_{\tau,L}(\mathbf{r} - \mathbf{R}) \tag{4}$$

where **R** represents the lattice vector in direct space, and τ and L have the same meaning as described above. By using (3) and (4), $\langle \mathbf{k}j|\mathbf{k}j\rangle = 1$ can be expanded as follows:

$$\langle \mathbf{k}j|\mathbf{k}j\rangle = \int d\mathbf{r} \sum_{\mathbf{R},\mathbf{R}',\tau,\tau',L,L'} e^{i\mathbf{k}(\mathbf{R}'-\mathbf{R})} \chi^*_{\tau,L}(\mathbf{r} - \mathbf{R}) \chi_{\tau',L'}(\mathbf{r} - \mathbf{R}') C_{\tau,L}^{\mathbf{k}j*} C_{\tau',L'}^{\mathbf{k}j} \tag{5}$$

By changing the variables $\mathbf{r} - \mathbf{R}$ as **r** and $\mathbf{R}' - \mathbf{R}$ as **R**, (5) can be rewritten as follows:

$$\langle \mathbf{k}j|\mathbf{k}j\rangle = \sum_{\tau,\tau',L,L'} \Big[\sum_{\mathbf{R}} \int d\mathbf{r} e^{i\mathbf{k}\mathbf{R}} \chi^*_{\tau,L}(\mathbf{r}) \chi_{\tau',L'}(\mathbf{r} - \mathbf{R})\Big] C_{\tau,L}^{\mathbf{k}j*} C_{\tau',L'}^{\mathbf{k}j} \tag{6}$$

The part in the bracket can be defined as the **k**-dependent overlap matrix element as

$$S_{\tau,\tau'}^{\mathbf{k}}(L,L') = \sum_{\mathbf{R}} e^{i\mathbf{k}\mathbf{R}} \int \chi^*_{\tau,L}(\mathbf{r}) \chi_{\tau',L'}(\mathbf{r} - \mathbf{R})\, d\mathbf{r} \tag{7}$$

By using (7), (6) can be written in a more compact form as follows:

$$\langle \mathbf{k}j|\mathbf{k}j\rangle = \sum_{\tau,\tau'} \sum_{L,L'} S_{\tau,\tau'}^{\mathbf{k}}(L,L') C_{\tau,L}^{\mathbf{k}j*} C_{\tau',L'}^{\mathbf{k}j} \tag{8}$$

Thus, the total probability of the $|\mathbf{k}j\rangle$ state electrons occurring in the entire space is partitioned into the on-site part ($\tau = \tau'$) and the intersite part ($\tau \neq \tau'$). The latter part can be used as a bonding indicator to measure the contribution of a specific state $|\mathbf{k}j\rangle$ to the bonding between atoms τ and τ':

$$B^{\mathbf{k}j}(\tau,\tau') = \sum_{L,L'} C_{\tau,L}^{\mathbf{k}j*} C_{\tau',L'}^{\mathbf{k}j} S_{\tau,\tau'}^{\mathbf{k}j}(L,L') \tag{9}$$

Obviously, $B^{\mathbf{k}j}(\tau,\tau')$ expresses essentially the same as COOP in partitioning the electrons. It should be noted that $B^{\mathbf{k}j}(\tau,\tau')$ is also basis set dependent and thus is not an absolute indicator. In fact, as the present bonding indicators do not correspond to quantum mechanical operators, they are not measurable quantities of a microscopic quantum system. For example, both COHP and TBB[18] depend on the approach to partition the total energy. The basis dependence of $B^{\mathbf{k}j}(\tau,\tau')$ as defined in (9) has some shortcoming; e.g., this bonding indicator cannot be used in the case of an orthogonal basis. Some other problems have been discussed in detail in ref 11. In practice, since $B^{\mathbf{k}j}(\tau,\tau')$ depends on the expansion coefficients $C_\tau^{\mathbf{k}j}(L)$, the corresponding wave functions must be normalized in the same way in order to compare the variation of the bonding indicators. And when τ and τ' are not in the same primitive unit cell, the corresponding coefficients and overlap integrals should be used by considering the Bloch law. At the present stage, it is still difficult to directly implement the above approach into the full potential LMTO (FP-LMTO) framework due to the fact that (i) the full potential LMTOs are long-ranged instead of tight-binding, (ii) the full potential LMTOs are not only **k**-dependent but also ϵ-dependent, where ϵ is an energy parameter to represent the tail energy of the envelop function. Such properties make the above electron partition ill-defined and the computation for the overlap matrix elements unnecessarily tedious. In this work, we approximate the overlap matrix elements in (5) by those obtained from the Slater basis. Such an approximation is acceptable as the extended Hückel bands[19] can be adjusted to the ab initio bands as we have shown in an earlier paper.[3]

The indicator $B^{\mathbf{k}j}(\tau,\tau')$ describes the bonding property of a state $|\Phi_{\mathbf{k}j}\rangle$ for atomic pairs (τ,τ'), so it can be used to describe the bonding property of an electronic state in a two-atom molecule. However, for multiatom molecules and solids, it cannot be used directly because the state $|\Phi_{\mathbf{k}j}\rangle$ involves many atoms. To describe the bond character of a multiatomic state, one needs to consider all of the pairs involved in this state.

(11) Dronskowski, R.; Blöchl, P. E. *J. Phys. Chem.* **1993**, *97*, 8617.
(12) Andersen O. K.; Jepsen, O. *Phys. Rev. Lett.* **1984**, *53*, 2571.
(13) Hughbanks, T.; Hoffmann, R. *J. Am. Chem. Soc.* **1983**, *105*, 3528.
(14) Hoffmann, R.; Lipscomb, W. N. *J. Chem. Phys.* **1962**, *36*, 2179.
(15) Hoffmann, R. *Angew. Chem., Int. Ed. Engl*. **l987**, *26*, 846.
(16) Savrasov S. Y.; Savrasov, D. Y. *Phys. Rev. B* **1996**, *54*, 16487.
(17) Mulliken, R. S. *J. Chem. Phys.* **1955**, *23*, 1833.
(18) Sutton, A. P.; Finnis, M. W.; Pettifor, D. G.; Ohta, Y. *J. Phys. C* **1988**, *21*, 35.
(19) Landrum, G. A. YAeHMOP: Another EHMO package, R. Hoffmann's group, Cornell University, 1997.

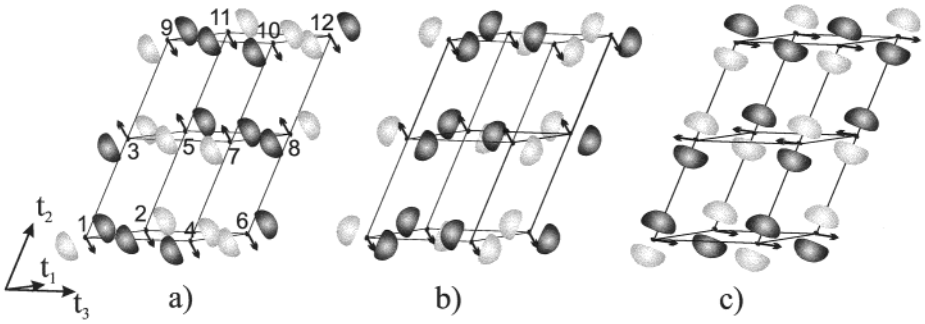

Figure 1. Projection of the orbitals of the (a) $|Z6\rangle$, (b) $|D6\rangle$, and (c) $|F6\rangle$ states of Hg together with the doubled unit cell and the $\mathbf{L}_1$ (a and b) and $\mathbf{L}_3$ (c) phonon patterns represented by arrows. The numbering for the Hg atoms is additionally given in (a).

Hence, we define a functional for an electronic state $|\Phi_{\mathbf{k}j}\rangle$ as follows:

$$\mathrm{Psib}(\Phi_{\mathbf{k}j}) = \sum_{\tau<\tau'} B^{\mathbf{k}j}(\tau,\tau')/N \qquad (10)$$

where the summation in the numerator is done over all pairs involved in a state $|\Phi_{\mathbf{k}j}\rangle$. The condition $\tau < \tau'$ guarantees that every pair is only counted once. N is the total number of such pairs. For solids, the summation poses no problem because only the pairs in the unit cell need to be considered due to the periodicity. Even in the nonperiodic case, the summation will terminate at limited terms, as $B^{\mathbf{k}j}(\tau,\tau')$ will become zero when the distance between τ and τ' exceeds some fixed value. $\mathrm{Psib}(\Phi_{\mathbf{k}j})$ is actually an algebraic average of the bonding indicators, and therefore, it not only contains the dominant bonding interactions but also considers the other weak interactions and the possible cancellations among them. Accordingly, we attribute the bond character of a state $|\Phi_{\mathbf{k}j}\rangle$ to $\mathrm{Psib}(\Phi_{\mathbf{k}j})$. It should be pointed out that as Mulliken's electron number partitioning scheme was used to determine $B^{\mathbf{k}j}(\tau,\tau')$, the approximations such as the basis set dependence and other problems[11] are inherited to $\mathrm{Psib}(\Phi_{\mathbf{k}j})$. However, as we are only interested in the variation of $\mathrm{Psib}(\Phi_{\mathbf{k}j})$, such approximations will not hurt our result too much.

Computational Details

Mercury has been chosen as an example to illustrate the response of a flat band state to phonons. On the basis of our preceding work,[5] we know that for Hg only the first branch phonons along the $\Gamma-L$ and $\Gamma-F$ directions of the first Brillouin zone (BZ) can effectively couple to the electronic states in the vicinity of the Fermi level. In this work, we have chosen the L_1 and the L_3 phonons, which couple strongly and weakly, respectively. The eigen vectors obtained from the linear-response calculations are $\mathbf{e}_{L1} = (0, -1, 0)$ and $\mathbf{e}_{L3} = (0.7884, 0, 0.6151)$ in Cartesian coordinates. They are plotted in Figure 1. which shows that the two phonon modes double the original primitive unit cell and modulate the structure in a different way. It is interesting to learn why they behave so drastically different in their coupling to the electrons and how they affect the flat band state.

By freezing the above two phonons, we obtain two superstructures (Hg-L_1, Hg-L_3) from the original rhombohedral structure of Hg. The electronic structures may be computed for these structures via various first-principles methods. In this work, the FP-LMTO[20] method based on the local-density approximation (LDA) of Janak−Moruzzi−Williams[21] exchange-correlation potential with a general gradient approximation (GGA) of Perdew et al.[22] has been employed, in which a potential of arbitrary shape instead of the atomic sphere approximation (ASA)[23] ensures the accuracy when dealing with phonons. Besides, the adiabatic approximation in dealing with the electron−phonon systems is assumed in this work. To conveniently calculate and represent some quantities in the interstitial region, the plane-wave Fourier representation is used in this region, which requires pseudo-Hankel functions instead of the singular Hankel functions to be taken as the envelop functions. Except for the structural parameters, all other computational parameters are the same for the three structures. The 2κ- 6s, 6p, 5d LMTO basis has been used for valence states, while the 5p state is treated as semicore state throughout this work. The one-center expansions inside the MT spheres are performed up to $l_{\max} = 6$. In the interstitial region, the pseudo-LMTOs are expanded in plane waves up to 9.63, 13.3, and 20.0 Ry, 9.62, 14.5, and 20.4 Ry, respectively, for 6s, 6p, 5d orbitals of Hg and Hg-L. The charge densities and the potentials inside the MT sphere are represented by the spherical harmonics up to $l_{\max} = 6$, while those in the interstitial region are represented by 2634 and 5266 plane waves, respectively, for Hg and Hg-L. The nontouching MT sphere radius is taken to be 2.82 and 2.76 au for Hg and Hg-L, respectively. The calculations have been carried out to self-consistency by using a $18 \times 18 \times 18$ k-mesh (580 independent k points for Hg, 5832 for Hg-L) and a modified tetrahedron method with a nonlinear instead of the usual linear interpolation.[24] All calculations are based on the primitive unit cell parameter $a = 5.6427$ au for Hg.

Results and Discussion

The phonon pattern of $L = {}^1/_2\mathbf{g}_2$ shown in Figure 1 has the Cartesian coordinates $(-1/6, {}^1/_2(3)^{1/2}, {}^1/_6 tg(\theta))2\pi/a'$, with $a' = a\sin(\theta)$, $\theta = 41.946°$, where $\mathbf{g}_2$ is one of the reciprocal unit cell basis vectors in $\mathbf{q}$ space. From Figure 1, it is obvious that the frozen L phonon results in a doubled unit cell along the $\mathbf{t}_2$ direction of the undistorted rhombohedral cell. Accordingly, the first Brillouin zone $(\mathrm{BZ})_o$ is reduced to half of the original one along the $\mathbf{g}_2$ direction. As shown in Figure 2, the D_{3d} symmetry of $(\mathrm{BZ})_o$ is completely broken by the L phonon, and the originally equivalent high-symmetry $\mathbf{k}$ points in part become unequivalent. The L point with a coordinate of $(0, {}^1/_2, 0)$ expressed in the reciprocal basis vectors $\mathbf{g}_1, \mathbf{g}_2, \mathbf{g}_3$ is transformed onto the Γ point in the new BZ, $(\mathrm{BZ})_L$, of the Hg-L structure, while the other L point at $({}^1/_2, 0, 0)$ becomes unequivalent to the former one. We call it B point. The F point at $({}^1/_2, {}^1/_2, 0)$ is also transformed onto this B point, while one of its equivalents at $({}^1/_2, 0, {}^1/_2)$ remains unmoved. We call it D point. The original Z point at $({}^1/_2, {}^1/_2, {}^1/_2)$ also transforms onto this D point. The other $\mathbf{k}$ points in the BZ are transformed in a similar way;

(20) Savrasov, S. Y. *Phys. Rev. B* **1996**, *54*, 16470.
(21) Janak, J. F.; Moruzzi, V. L.; Williams, A. R. *Phys. Rev. B* **1975**, *12*, 1257.
(22) Perdew, J. P.; Burke, K.; Ernzerhof, M. *Phys. Rev. Lett.* **1996**, *49*, 3865.
(23) Perrot, F. *Phys. Status Solidi B* **1973**, *60*, 223.
(24) Blöchl, P.; Jepsen, O.; Andersen, O. K. *Phys. Rev. B* **1994**, *49*, 16223.

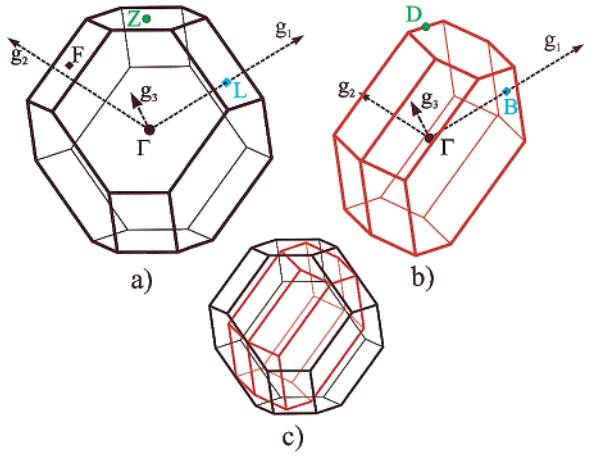

Figure 2. Projections of the first Brillouin zones (a) $(BZ)_o$ of Hg and (b) $(BZ)_L$ corresponding to Hg distorted by the frozen **L** phonons and (c) $(BZ)_L$ inserted into $(BZ)_o$ for direct comparison.

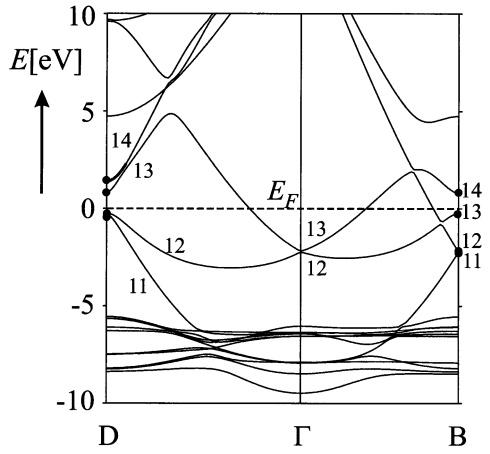

Figure 3. Band structure of Hg distorted by the frozen L_1 phonon along selected symmetry lines calculated by the full potential LMTO method. (See also Figure 2b.)

however, we will focus on the *F* and *Z* points, because only these two **k** points in the irreducible wedge of the BZ have flat bands at the Fermi level.[3] Due to the distortions of the structure caused by the L_1 and L_3 phonons, the original degeneracy of bands at the special **k** points as described above is removed. This effect is expected to be very small considering the energy scale of phonons (Debye frequency) in comparison with that of the electrons (Fermi energy). For this reason, as an illustration we only have plotted the band structures of Hg-L_1 in Figure 3, which shows that the two flat bands at *D* stem from the *F* (upper) and *Z* point (lower) in $(BZ)_L$, respectively, while the flat band at the *B* point is attributed to the *F* point. The electronic states that lie in the original $(BZ)_o$ but outside of $(BZ)_L$ are all folded into the latter, a fact that increases the number of bands as compared to the band structure of undistorted Hg; see Figure 3. For some special **k** points, the eigenvalues relative to the Fermi energies and their changes caused by the corresponding phonons are listed in Table 1. Also shown are the relations between the electronic states in $(BZ)_o$ and $(BZ)_L$. For example, the $|L7\rangle$ state (*L* is the **k** point and 7 refers to the band index) scatters via the L phonon to the $|\Gamma 13\rangle$ state. The identities between the eigenvalues of $|L\rangle$ and $|B\rangle$ and those of $|D\rangle$ and $|F\rangle$ in undistorted Hg are simply the result of symmetry. As shown in column $\Delta 1$ and $\Delta 2$, the mean values of the changes of the eigenvalues with respect to the Fermi level are 0.001 73 (0.023 57 eV) and 0.00 167 Ry (0.022 71 eV) for L_1 and L_3 phonons, respectively. Provided the electron pairing is mediated by the phonons, the pairing energy is in the order of ~0.02 eV, a value that is consistent with the experimental and theoretical findings. The fact that the mean value of the $\Delta 1$ column is larger than that of the $\Delta 2$ column indicates a more effective coupling of the L_1 phonon with the electrons compared to the L_3 phonon in agreement with our earlier results of electron−phonon coupling constant distribution in **q** space.[5] Another interesting fact concerns both the negative and the positive values occurring in the $\Delta 1$ and $\Delta 2$ columns, which implies that with the mediation of phonons the electronic states very close to the Fermi level can fluctuate around the Fermi level, provided the Fermi energy is not affected by the electron−phonon interaction. The latter assumption can be verified by calculating the electron−phonon self-energy at low temperature.[25] It needs to be pointed out that $\Delta 1$ and $\Delta 2$ as defined in Table 1 reflect the second-order and higher effect of a phonon on an electronic state because the first-order variation of the eigenvalue should be zero.[5,20] As far as the electron−phonon matrix element is concerned, they reflect part of the electron−phonon coupling. This can be seen by approximating the two splits:[26] $\tilde{\epsilon}_{\mathbf{k}n} - \tilde{\epsilon}_{\mathbf{k}+\mathbf{q}m}$ and $\epsilon_{\mathbf{k}n} - \epsilon_{\mathbf{k}+\mathbf{q}m}$ of "degenerate" Fermi states $|\mathbf{k}n\rangle$ and $|\mathbf{k}+\mathbf{q}m\rangle$ with $2(\tilde{\epsilon}_{\mathbf{k}n} - \tilde{\epsilon}_F)$ and $2(\epsilon_{\mathbf{k}n} - \epsilon_F)$, respectively, for the distorted and undistorted structure. Through this substitution, the square electron−phonon matrix element $(\Delta\tilde{\epsilon}^2 - \Delta\epsilon^2)/4$ in ref 26 reduces to $(|\tilde{\epsilon}_{\mathbf{k}n} - \tilde{\epsilon}_{\mathbf{F}}| - |\epsilon_{\mathbf{k}n} - \epsilon_{\mathbf{F}}|)\,(|\tilde{\epsilon}_{\mathbf{k}n} - \tilde{\epsilon}_{\mathbf{F}}| + |\epsilon_{\mathbf{k}n} - \epsilon_{\mathbf{F}}|)$. Obviously our $\Delta 1$ and $\Delta 2$ correspond to the content in the first parentheses. In ref 26, $\tilde{\epsilon}_{\mathbf{k}n}$, $\epsilon_{\mathbf{k}n}$, etc., are all obtained through interpolations, respectively based on the distorted and undistorted structure, while in our case $\tilde{\epsilon}_{\mathbf{k}n}$ and $\epsilon_{\mathbf{k}n}$ are all eigenvalues close to the Fermi level.

The relatively large differences among the Fermi energies (see Table 1) can be attributed to the fact that the frozen phonon approach treats the phonon affected structure as a statically different structure, which is obviously a drawback of this approach. However, the quantities in Table 1 are all relative ones to the corresponding Fermi energies, so the drawback mentioned above is well overcome.

We thus give numerical evidence to our earlier speculation that the flat band state at the Fermi level can be dynamically emptied and filled due to lattice vibrations[3]. As shown in Table 1, among the flat band states close to the Fermi level, the state $|Z6\rangle$ is most effectively coupled to the L_1 phonon, the next is $|D6\rangle$, while the state $|F6\rangle$, which is equivalent to $|D6\rangle$, is the least. Such differences between the effects of L_1 and L_3 phonons and the resulting changes to the different flat band states can be explained reasonably well by investigating the bonding property and its variation during the electron−phonon interaction process. In Table 2, we list the calculated values of Psib(Φ) as defined in this work for the flat band states of Hg and their variations. The identity of the numerical values for Psib(D_6) and Psib(F_6) is of no surprise as they refer to actually equivalent states in the rhombohedral structure of Hg. Our calculation indicates that $|Z6\rangle$ is a pure p_z state, while $|F6\rangle$ and $|D6\rangle$ are

(25) Butler, W. H. *Treatise on Materials Science and Technology*; Fradin, F. Y. Ed.; Academic Press: New York, 1981; Vol. 21, p 165.
(26) Liechtenstein, A. I.; Mazin, I. I.; Rodriguez, C. O.; Jepsen, O.; Andersen, O. K. *Phys. Rev. B* **1991**, *44*, 5388.

Table 1. Eigenvalues (Ry) and Their Changes at Some **k** Points[a]

Hg-0 $E_F = 0.557\ 13$	Hg-L_1 $E_F = 0.585\ 44$		Hg-L_3 $E_F = 0.584\ 14$	
$\Delta E(\mathbf{k}j)$	$\Delta E(\mathbf{k}j)$	$\Delta 1$	$\Delta E(\mathbf{k}j)$	$\Delta 2$
−0.157 65 (L_7)	−0.158 50 (Γ_{13})	0.8452×10^{-3}	−0.159 02 (Γ_{13})	0.1370×10^{-2}
−0.162 07 (L_6)	−0.163 78 (Γ_{12})	0.1710×10^{-2}	−0.163 45 (Γ_{12})	0.1380×10^{-2}
0.103 53 (Z_7)	0.102 53 (D_{14})	-0.9998×10^{-3}	0.101 08 (D_{14})	-0.2440×10^{-2}
−0.017 93 (Z_6)	−0.020 78 (D_{11})	0.2840×10^{-2}	−0.019 37 (D_{11})	0.1440×10^{-2}
0.061 97 (D_7)	0.060 89 (D_{13})	-0.1080×10^{-2}	0.059 91 (D_{13})	-0.2060×10^{-2}
−0.016 00 (D_6)	−0.018 63 (D_{12})	0.2620×10^{-2}	−0.017 45 (D_{12})	0.1450×10^{-2}
−0.157 65 (B_7)	−0.159 68 (B_{12})	0.2030×10^{-2}	−0.159 57 (B_{12})	0.1920×10^{-2}
−0.162 07 (B_6)	−0.164 74 (B_{11})	0.2670×10^{-2}	−0.163 85 (B_{11})	0.1790×10^{-2}
0.061 97 (F_7)	0.059 83 (B_{14})	-0.2150×10^{-2}	0.060 03 (B_{14})	-0.1940×10^{-2}
−0.016 00 (F_6)	−0.016 38 (B_{13})	0.3740×10^{-3}	−0.016 91 (B_{13})	0.9025×10^{-3}

[a] E_F is the Fermi energy, $\Delta E(\mathbf{k}j) = E(\mathbf{k}j) - E_F$, $\Delta 1 = |\Delta E(\mathbf{k}j)$ of Hg-L1$| - |\Delta E(\mathbf{k}j)$ of Hg-0$|$, $\Delta 2$ is defined similarly to $\Delta 1$. After each value, the **k** point and band index in the corresponding BZ is given in parentheses.

Table 2. Values of Psib(Φ) $\times 10^2$ for the Flat Bands of Hg and Their Variations Caused by the Phonons L_1 and L_3[a]

Hg-0	Hg-L_1		Hg-L_3	
Psib (Φ)	Psib (Φ)	ΔPsib	Psib (Φ)	ΔPsib
1.3754 (Z_6)	1.0923 (D_{11})	−0.2831	1.2246 (D_{11})	−0.1508
1.2964 (D_6)	1.0229 (D_{12})	−0.2735	1.1490 (D_{12})	−0.1474
1.2964 (F_6)	1.0462 (B_{13})	−0.2502	1.1575 (B_{13})	−0.1389

[a] The ΔPsib values are calculated as Psib(Φ_2) − Psib(Φ_1), where Φ_1 represents the initial state as in the first column, while Φ_2 is the final state.

hybrids of $0.2574p_x + 0.4349p_y + 0.4946p_z$, and $0.2574p_x - 0.4349p_y + 0.4946p_z$, respectively. This difference in combination with the phase change required by the Bloch law decides the bonding difference between these states. For example, due to the pure p_z character, the bonding property of $|Z6\rangle$ is isotropic, namely. $B(1,2) = B(1,3) = B(1,4)... = 0.531 \times 10^{-1}$ (first nearest neighbors (nn)); $B(2,3) = B(2,4) = B(3,4)... = 0.75 \times 10^{-2}$ (second nn); $B(2,7) = B(3,6) = B(4,5) = 0.85 \times 10^{-3}$ (third nn); $B(1,5) = B(1,6) = B(1,7)... = -0.185 \times 10^{-2}$ (fourth nn). While those for the $|F6\rangle$ are very anisotropic, e.g., in the case of first nn $B(1,2) = 0.5711 \times 10^{-1}$, $B(1,3) = 0.5529 \times 10^{-1}$, $B(1,4) = 0.2131 \times 10^{-1}$, ... Obviously, it is the mixing of p_x and p_y into p_z that reduces the overlap of the relevant orbitals of $|F6\rangle$ and $|D6\rangle$ and thus weakens their bonding properties as indicated by Psib($|F6\rangle$) and Psib($|D6\rangle$) in Table 2. The most interesting fact in Table 2 is that all of the absolute values of ΔPsib(Φ) for the L_1 phonon are larger than those for L_3 phonons. This fact implies that the L_1 phonon causes stronger electron−phonon interactions, which produce a larger change of the bonding property of an electronic state as indicated by the value of Psib(Φ). In our present approach, the changes of the functional Psib(Φ) arise from mainly two sources. The first one concerns the changes of the overlap integrals caused by the static distortion of the structure, which enters into Psib(Φ) through formulas 5 and 6. The second one is due to the change of the wave function. For example, from $|Z6\rangle$ to $|D11\rangle$, the wave function changes from a pure p_z state to a hybrid state of s, p, and d waves, which will result in new terms in the calculation of $B^{\mathbf{k}j}(\tau,\tau')$ in (5) and thus changes the value of Psib(Φ). Obviously, the former one reflects the way a phonon distorts a structure, while the latter one reflects how an electronic state responds to this distortion. As shown in Figure 1, the L_1 phonon should couple to the corresponding states more strongly than the L_3 phonon because it can stretch the bonds more effectively than the L_3 phonon according to their displacement patterns. The larger variation of Psib($|D6\rangle$) as compared to that of Psib($|F6\rangle$) shown in Table 2 can easily be explained by inspecting their orbital topology and the phonon pattern as shown in Figure 1. It is obvious that both L_1 and L_3 phonons mainly affect the bonding along the $\mathbf{t}_2$ direction; however, for $|F6\rangle$, that direction is associated with stronger bonding due to stronger overlap ($B(1,3) = 0.5529 \times 10^{-1}$), while for $|D6\rangle$, it is weaker ($B(1,3) = 0.2131 \times 10^{-1}$). Therefore, both the L_1 and L_3 phonons will hardly distort $|F6\rangle$. The larger variation of Psib($|Z6\rangle$) compared to Psib($|D6\rangle$) cannot be explained by only considering the first-order bonding interaction as before, because $B(1,3) = 0.531 \times 10^{-1}$ of $|Z6\rangle$ is even larger than that of $|D6\rangle$ (0.2131×10^{-1}). However, the second order Psib($|Z6\rangle$) is much smaller (0.75×10^{-2}) than that of $|D6\rangle$ (0.1321×10^{-1}), and so is the third order Psib value. Besides, since $|Z6\rangle$ is a pure p_z state, the contribution of wave function variations to this state as discussed above is larger than that of $|D6\rangle$. These factors combine to produce a larger variation of Psib($|Z6\rangle$) than that of Psib($|D6\rangle$). In fact, higher order Psib(Φ) should play a more important role than the first order Psib(Φ) in deciding the variations, because normally the phonon energy is not high enough to influence the first nn bonding.

On the basis of the above discussions, we give a rational explanation for the flat band states having electron−phonon coupling strengths according to $|Z6\rangle > |D6\rangle > |F6\rangle$ as shown in Table 1. It should be noted that in this work the electron−phonon coupling has been discussed based on the quantity (ΔE_{kj}), which is related to the "electron−phonon matrix elements" as discussed above. Though the electron−phonon matrix element is of greatest importance among the factors[27] that influence the electron−phonon coupling constant λ as used by physicists, it is generally necessary to consider the geometrical structure of the Fermi surface and the Fermi velocities in order to get a full understanding of the peaklike structure of λ in **q** space. The reason for the necessity to include the "geometrical effect" and the "velocity effect" is because $\lambda(\mathbf{q})$ contains all the contributions of the electronic states that are related by **q**. For Hg, as there is no flat sheet on the Fermi surface and no structure for the density of states at E_F, these two effects should be even smaller than those in Nb.[25] Therefore, the change of Psib(Φ) that indicates the matrix element effect can reveal the origin of the peaklike structure of λ in **q** space for Hg[5].

(27) Butler, W. H.; Smith, H. G.; Wakabayashi, N. *Phys. Rev. Lett.* **1977**, *39*, 1004.

In summary, the frozen phonon approach has been used to study the electronic structure of Hg. By introducing a new functional Psib(Φ), we have provided a chemical approach to explain the coupling between a specific electronic state and a specific phonon. The approximations in the calculations of Psib(Φ) can be improved by using energy partitioning scheme in calculating $B^{\mathbf{k}j}(\tau,\tau')$ and thus to put the whole calculations in one frame. This will be left to our future work.

Acknowledgment. The authors thank Dr. O. Jepsen for critical comments and helpful discussions.

JA011815Q